Editors' Suggestion

Effect of adhesion on material removal during adhesive wear

Ramin Aghababaei*
Engineering Department, Aarhus University, 8000 Aarhus C, Denmark
and Center for Integrated Materials Research (iMat), Aarhus University, 8000 Aarhus C, Denmark

(Received 4 March 2019; published 11 June 2019)

The process of surface degradation and material removal due to adhesive force between rubbing surfaces (i.e., adhesive wear) involves an apparent contradiction. The material exchange between sliding surfaces requires a strong adhesion between surface asperities, whereas the detachment of final wear particles demands a weak adhesion between worn fragments and sliding surfaces. Here, using a coarse-grained numerical technique, we study the complete process of wear particle formation (i.e., nucleation, evolution, and detachment) during adhesive sliding contact. We show that discrepant experimental and theoretical wear observations can be attributed to different stages of the wear particle formation. In particular, we address the opposite contribution of adhesion into the formation and detachment processes of wear particles. Our simulations reveal that reducing adhesion diminishes the adhesive wear in three ways: (i) reducing the probability of wear particle formation, (ii) increasing the required energy per unit volume of removed materials (i.e., decreasing the energy efficiency for particle formation), and (iii) alleviating the growth of formed wear fragments.

DOI: 10.1103/PhysRevMaterials.3.063604

I. INTRODUCTION

Adhesive wear is the process of surface material removal due to localized adhesive bonds between sliding surfaces. The degree of interfacial adhesion between contacting surfaces is controlled by several factors such as environmental conditions [1–3], the degree of surface chemical contamination [4–8], material compatibility/solubility [2], and surface roughness [9–14]. It has been empirically shown that one can diminish adhesive wear by reducing the strength of interfacial adhesion between sliding surfaces [15–17]. A clear mechanistic picture of adhesion contribution into the material removal process, however, remain elusive as most wear observations are obtained from post-factum analysis of worn surfaces.

It has long been hypothesized [18,19] that during adhesive contact between two solid surfaces, a small fraction of surface asperities contact at their tip, forming strong adhesive junctions resulting from the cold welding process. During sliding, a negligible fraction of these junctions fails under combined compressive-shear stress state, leading to material transfer between sliding surfaces [20,21]. Several mechanisms such as subsurface crack propagation [22,23], surface material delamination [24,25] and ploughing mechanisms [26] have been proposed for the process of material removal during sliding wear. Detailed microscopic analysis [1,5,24] suggested that transferred fragments grow by continuous removal of additional surface material and agglomeration with other fragments. These fragments may eventually be eliminated from the contact in the form of loose wear particles [1].

The examination of wear particle morphology (e.g., size, shape, and structure) at different stages of wear processes can reveal valuable information about wear mechanisms and influencing factors [27–29]. Three stages have been distingiushed in the life of an adhesive wear particle [1,30,31]: (i) material transfer between sliding surfaces, (ii) wear particle formation through growth and agglomeration of transferred fragments, and (iii) wear particle matureness (i.e., steady state rolling or elimination out of the contact).

A clear understanding of these hypotheses and influencing parameters necessitates an in-situ microscopic tracking or direct simulation of the process of wear particle formation, which presents notorious experimental [32] and numerical [33–36] challenges.

Recent numerical simulations [9,37–39] showed that a wear fragment forms at the onset of contact between two asperities, only if the junction between the two asperities, is bigger than a characteristic length scale. Comparing the stored elastic energy at the asperity junction and the fracture energy associated with the nucleation and propagation of subsurface cracks at the asperities base, the model [9] provides a critical junction size as a function of shear modulus (μ) and fracture energy (G) of the contacting asperities and the interfacial shear strength of the junction (τ_j):

$$d_j = \lambda \frac{\mu G}{\tau_j^2}, \tag{1}$$

where λ is a shape factor, which equals to $8/\pi$ and 3 for idealized cases of cylindrical and spherical particle formation respectively. For brittle materials, the fracture energy can be estimated as twice of the surface energy [40], whereas for ductile materials, additional contribution due to plastic dissipation needs to be considered in the fracture energy [41]. Equation (1) predicts a critical junction size (d_j) for the asperity fracture and wear fragment formation at the asperity level adhesive contact. In other words, the more brittle the contacting asperities are, and if the interfacial adhesion is stronger, the minimum junction size for fragment generation

*aghababaei@eng.au.dk

will be smaller. The model has been extended for studying adhesive wear of sliding contact between rough surfaces [42,43] and slipping mechanism between interlocking asperities [44].

It has been argued [1,45] that wear fragments formed at the onset of contact between surface asperities are small and tightly adherent and they only come off in the form of larger particles by accretion of further material from sliding surfaces (i.e., snowball growth mechanism). The eventual detachment of wear particles from sliding surfaces has also been rationalized on the basis of adhesion reduction due to surface contamination [30,46] and/or the imperfection in the contact [47].

Rabinowicz [48–50] argued that an already formed fragment can come off as a loose wear particle if the internal energy stored into the adhered fragments exceeds the adhesive energy. Using this argument and assuming that only 10% of the maximum stored energy at yield can be trapped into an adhered fragment, he formulated a criterion for a minimum size of loose wear particles

$$d_p = \frac{30EW}{\sigma_{yp}^2}, \tag{2}$$

where E and σ_{yp} represent Young's modulus and the yield strength of the fragment and W is the work of adhesion. The work of adhesion at the interface between two solid surfaces can be defined as $W = \gamma_a + \gamma_b - \gamma_{ab}$, where γ_a and γ_b are the surface free energy of solid bodies a and b and γ_{ab} the interface free energy, all per unit area (for two identical solids, the work of adhesion is $W = 2\gamma_a$). Equation (2) estimates the minimum size of wear particles (d_p) over which adhered fragments come off as loose wear particles while smaller ones remain adherent.

While both models are developed based on the energy balance concept [40], the contribution of adhesion in them seems contradicting. In Eq. (1), decreasing adhesion reduces the shear strength of junction (τ_j) and therefore increases the critical junction size for nucleation of wear fragments. However, reducing adhesion causes a lower work of adhesion (W) in Eq. (2) and decreases the minimum size of loose wear particle. In other words, Rabinowicz's model [48] suggests a direct correlation between the interfacial adhesion and the size of loose wear particles, whereas the critical junction size model [9] suggests an inverse correlation between the interfacial adhesion and the minimum asperity junction size for wear particle formation.

Using a new numerical development, in this study, we investigate the contribution of adhesion in the nucleation, evolution and detachment processes of adhesive wear particles. Our simulations explain the opposite contribution of adhesion in the nucleation and evolution of wear particles during adhesive contact. Furthermore, the influence of interfacial adhesion on internal morphology of loose wear particles is discussed.

II. METHOD

All simulations are 2D molecular dynamics simulations performed in LAMMPS [53] using a recently developed coarse-grained model interatomic potential [9], which enables direct analysis of the wear particle formation at computationally feasible length scales [37,38]. The simulation setup is similar as in Ref. [9] [see Fig. 1(a)] i.e., sliding simulations with two pairs of colliding asperities and with a constant per atom normal load 0.001 ε/r_0 and constant tangential velocity 0.01 r_0/t_0 (t_0 is the reduced time unit) on a fixed layer on the top. Periodic boundary conditions are applied in the sliding direction. This idealized setup allows well-defined parametric studies that are impossible with more realistic surface geometries, while retaining the essential physics of the process. Throughout the paper, reduced units of ground-state bond length r_0 and bond energy ε are used. A Verlet algorithm with a time step $0.0025t_0$ is used for numerical integration. Langevin thermostats (with a damping parameter $0.05t_0$) at

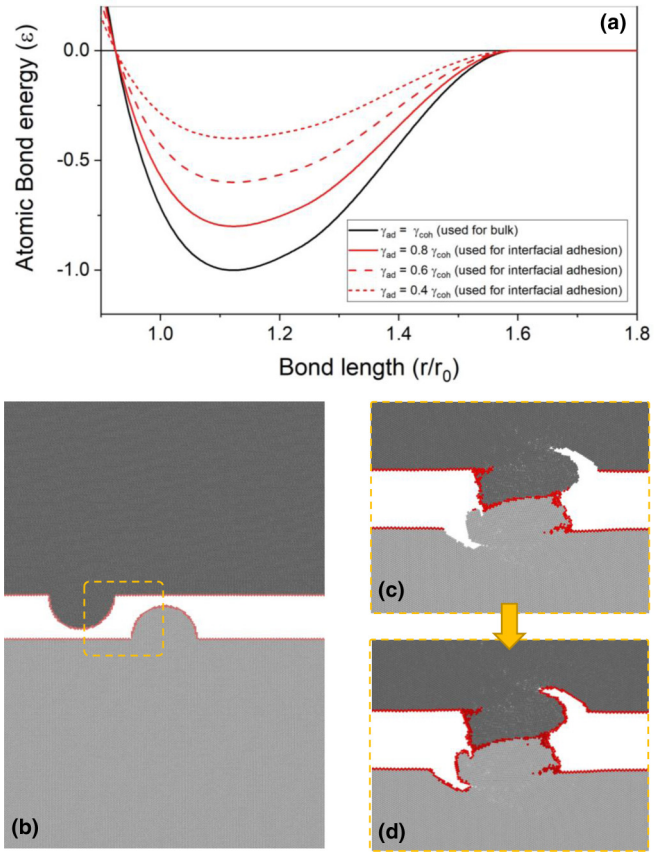

FIG. 1. (a) Bulk and interfacial interatomic potentials, used in this study. The cut off radius is reduced by modifying the tail of the Morse potential [51], to embrittle the system and to allow simulating the crack nucleation and propagation at the atomic level [9]. To model adhesion, a similar set of potentials with the bond energy differing by a scalar (0.4–1) is used. This factor, referred to the adhesion coefficient, represents the degree of interfacial adhesion with respects to the cohesion strength of sliding solids (i.e., $\gamma_{\text{adh}}/\gamma_{\text{coh}}$). (b) The idealized setup for simulating the wear particle formation at the asperity level adhesive contact. See Refs. [37,38] for more information about the simulation setup. Bulk and surface atoms are coloured in gray and red, respectively. While a same bulk potential is applied, two gray colors are used to distinguish the top and bottom solids. (c) and (d) show the result of a new algorithm that enables on-the-fly detection of surface atoms and reassignment of a weaker adhesion potential for modeling the effect of adhesion reduction due to surface contamination. See Sec. II for more information about the algorithm.

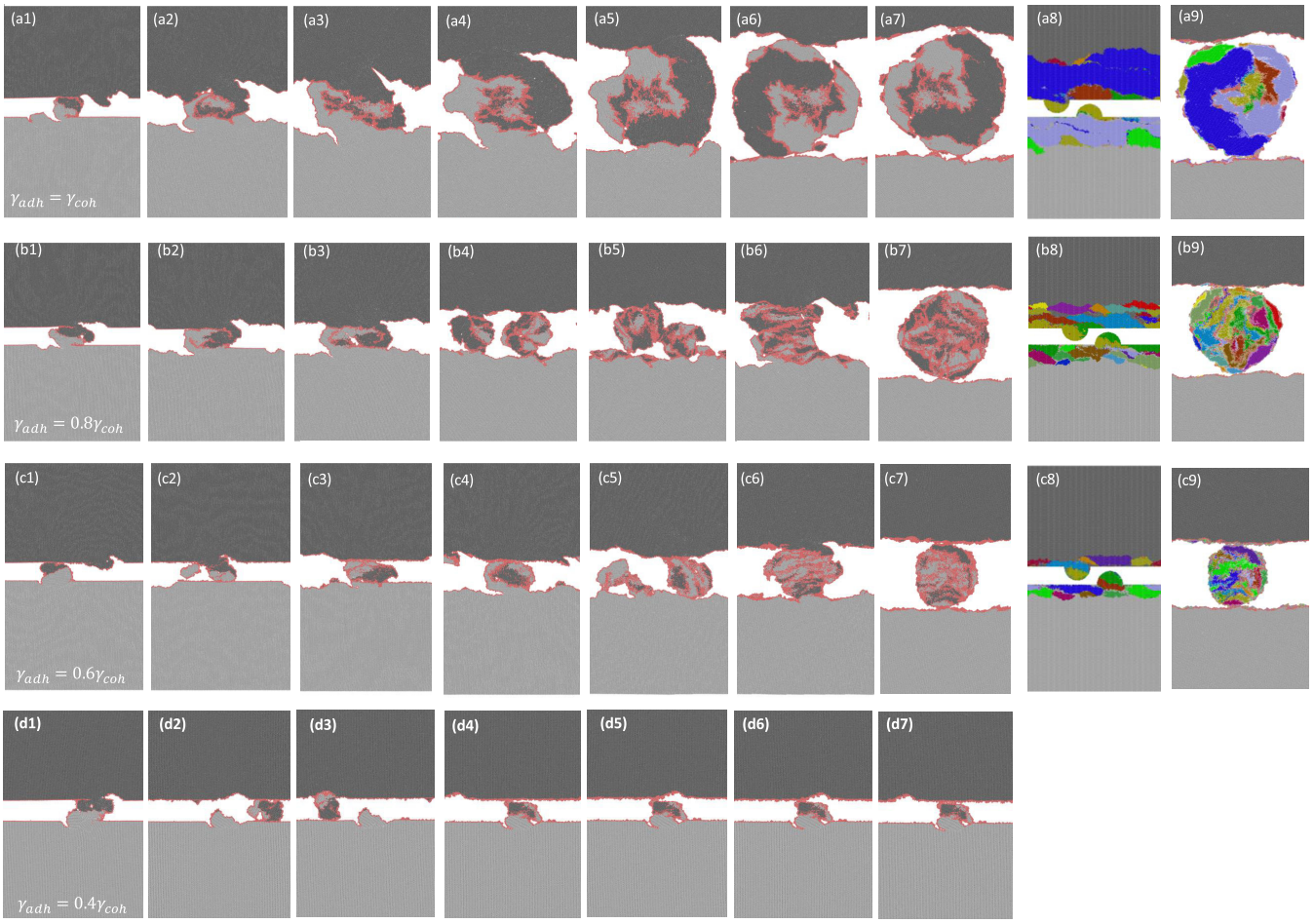

FIG. 2. Snapshots of different stages of wear particle formation in the presence of different interfacial adhesion: (a) $\gamma_{\text{adh}} = \gamma_{\text{coh}}$, (b) $0.8\gamma_{\text{coh}}$, and (c) $0.6\gamma_{\text{coh}}$. As shown in (d), no particle is formed with a lower interfacial adhesion $\gamma_{\text{adh}} = 0.4\gamma_{\text{coh}}$. The morphology of individually removed fragments during the process of wear particle formation in the reference and final configurations are shown in (a8), (a9), (b8), (b9), (c8), and (c9). An isolated fragment is identified when an area is entirely closed by surface atoms. See movie of these simulations in Ref. [52].

the boundaries were set to a temperature of $0.1\ \varepsilon/kB$. Analysis and visualization are conducted with OVITO [54].

To mimic the effect of interfacial adhesion, we use a similar set of potentials with the bond energy differing by a scalar (0.4–1) [see Fig. 1(a)]. This factor, referred to the adhesion coefficient in this study, represents the degree of interfacial adhesion with respects to the cohesion strength of sliding solids (i.e., $\gamma_{\text{adh}}/\gamma_{\text{coh}}$). To study the effect of adhesion at all stages of wear particle formation (and not only at the onset of asperity contact [37], Fig. 1(b)), we use a new numerical development to enable on-the-fly detection of surface atoms and re-assigning a specific interfacial adhesion potential to them [see Figs. 1(c) and 1(d)]. The method computes the atom coordination number considering the cutoff radius of $2.5r_0$ at every 1000 time step. Atoms with the coordination number between 0–15 are considered as surface/contaminated atoms. The coordination number for a bulk atom in a 2D hexagonal lattice with a cut off radius of 2.5 is 18. Next, we modify the interaction between those identified surface atoms for the remaining simulation time by changing the interatomic potential to a specific interfacial potential [see Fig. 1(d)]. This development also allows us to distinguish between inter- and intrafragment regions in a wear particle, revealing information about material removal mechanisms that contribute to the particle formation.

III. RESULTS AND DISCUSSION

Figure 2 presents snapshots of wear particle formation during sliding contact between two surfaces with the same initial surface topology (two semicircular asperities), material properties, sliding velocity and applied normal force, but different interfacial adhesion: $\gamma_{\text{adh}} = \gamma_{\text{coh}}$ [Fig. 2(a)], $\gamma_{ad} = 0.8\gamma_{\text{coh}}$ [Fig. 2(b)], and $\gamma_{\text{adh}} = 0.6\gamma_{\text{coh}}$ [Fig. 2(c)]. As seen, the nucleated wear fragment rolled over into a circular wear particle, where the system reaches to a steady state rolling condition. Similar observations have been reported in ceramics [55] and rock [56,57] friction experiments, where wear fragments agglomerate into cylindrical rolls by a shear-induced torque between the opposing slipping surfaces.

Interestingly, Fig. 2 demonstrates that the lower the adhesion, the smaller the final size of wear particle at the steady rolling state, which agrees with previous experimental observations [5,48,58] and the Rabinowicz's

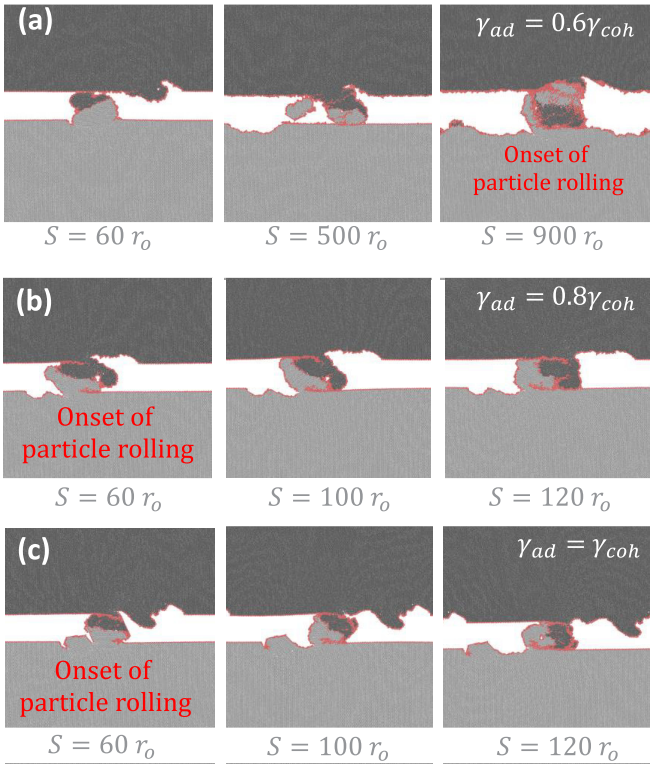

FIG. 3. The onset of snow ball particle growth mechanisms for different adhesion cases. Tracking the rotation of the interface line between the contacting asperities, it can be seen that the particle rolling is initiated at different stages of sliding for different adhesion parameters. (a) In the presence of low adhesion ($\gamma_{adh} = 0.6\gamma_{coh}$), wear particle rolling occurs after several contact events, once the size of the junction between the sliding surfaces becomes larger than the critical junction size required to form a particle. The particle formation, however, occurs at the first contact for higher adhesion parameters [(b) and (c)]. It can be seen that the higher the adhesion parameter, the smaller the wear particle at the onset of rolling. The onset of rolling is identified when the interface line between two asperities starts to rotate.

model [2]. On the other hand, consistent with the critical junction size model, Figs. 3(a)–3(c) show that the larger is the adhesion, the larger is the junction size to initiate snow ball growth mechanism.

As seen in Figs. 2(a1)–2(a7), if full adhesion presents ($\gamma_{adh} = \gamma_{coh}$), the initial contact between asperities forms a large and strong enough junction [Fig. 2(a1)]. The strong adhesion between asperities stimulates the shear strength of the junction and consequently reduces the critical junction size for the fracture-induced material removal [Eq. (1)]. The strong adhesion also expedites the formation process of wear particle via a few but severe removal of surface materials through deep subsurface cracking. In this situation, the imposed tangential work is mainly consumed to nucleate and propagate subsurface cracks. As a result, the final wear particle consists of a few large powderlike fragments with the same crystalline structure as the sliding solids. The morphology of removed fragments during the initial and final configurations are shown in Figs. 2(a8) and 2(a9), respectively.

Decreasing interfacial adhesion, however, increase the critical junction size for fragment nucleation via the asperity fracture [i.e., the larger junction is needed to remove surface material by fracture, Eq. (1)]. Considering the simulation with the adhesion coefficient of 0.6 [Figs. 2(c1)–2(c7)], it can be seen that first few contacts between asperities fail plastically without generating a fragment [Fig. 4(a)], as the initial asperity junction is smaller than the critical one. Further sliding results in further plastic deformation and material exchange between sliding surfaces which modifies the roughness of surfaces. Eventually, a fragment is nucleated at a later stage [Fig. 2(c3)], once the established junction between surfaces becomes larger than the critical junction size. For the 0.4 adhesion coefficient, the surface roughness is initially modified due to the lateral contact between the asperities, but soon the system reaches a steady state sliding condition without wear particle formation for the given applied load and boundary conditions.

Consistent with previous experimental observations [22,59], these simulations show that the lower the interfacial adhesion, the more gradual and mild the propagation of shallow subsurface cracks. As a result, the formed wear particle has a layered structure consisting of a more number of thin flakelike sheets with a large fraction of contaminated area between fragments.

It can also be seen that the weak inter-fragment adhesion causes disintegration of the rolling wear particle into smaller pieces (see Figs. 2(b3) and 2(c5) and movies in Ref. [52]). However, because of the imposed periodic boundary conditions in the simulation (i.e., mimicking reciprocal or cyclic sliding), broken fragments interact again and reagglomerate into a rolling particle [Figs. 2(b5) and 2(c6)].

To understand the micromechanics of material removal process and adhesive particle formation, we quantitatively analyze the energy efficiency of wear particle formation and the size and structural evolution of wear particles. Figures 4(a)–4(c) shows the evolution of tangential force (F), tangential work ($W = \int F ds$), and the volume of wear particles (V_p). It can be seen that the stronger the adhesion, the larger the maximum tangential force and the shorter the effective sliding distance (i.e., the sliding distance required to reach a steady state rolling condition). In other words, in the presence of strong adhesion, the debris particle forms by the agglomeration of a few but large fragments over a short sliding distance. In this simulation, a large portion of the wear particle volume (~50%) is removed as a result of one removal event [see Fig. 4(d)]. On the contrary, in the simulation with a weaker interfacial adhesion, a larger number of smaller fragments agglomerates over a longer sliding distance and forms a loose rolling wear particle [Fig. 4(d)].

Comparing the energy efficiency of the particle formation process (i.e., required energy per unit volume of removed material, W/V_p) in Fig. 4(d), it can be seen that the formation of a particle is less efficient in the presence of weak adhesion (i.e., a larger portion of tangential work dissipates through other mechanisms, e.g., frictional slipping, plasticity, and surface chemical contamination). Figure 4(f) confirms this argument by showing the percentage of contaminated atoms (i.e., atoms which being part of free/crack surfaces) inside wear particles. It shows that while this fraction is 20% in the presence of full

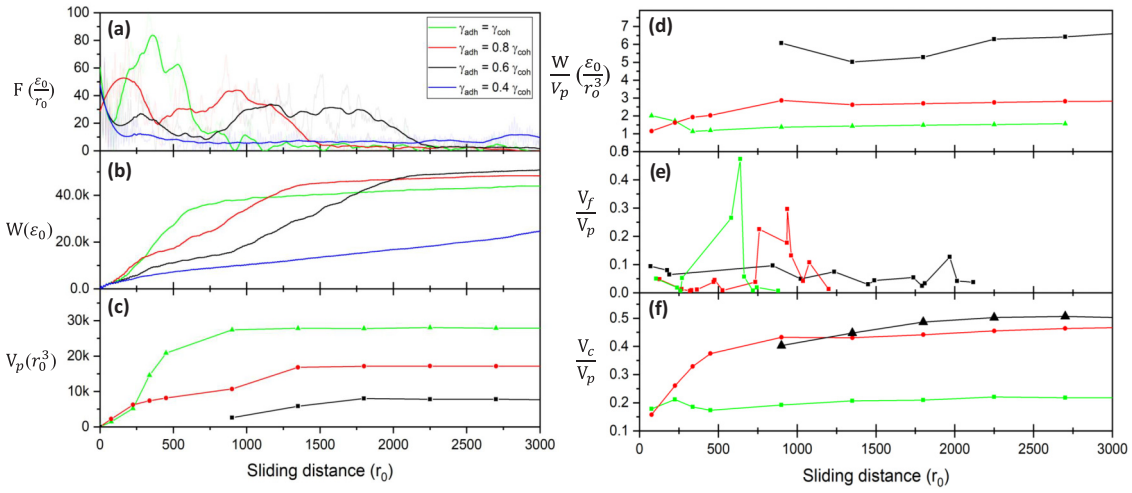

FIG. 4. Quantitative analysis of the evolution of (a) tangential force F, (b) energy W, (c) the particle volume V_p, and (d) the required energy per unit volume of removed material W/V_p. (e) presents the volume of individual wear fragment (V_f), normalized by the total volume of the particle at steady rolling state. (f) shows the fraction of contaminated surface atoms (i.e., atoms which being part of free/fracture surfaces) inside the formed wear particles ($V_c V_p$). The unit thickness is assumed for volume quantities.

adhesion ($\gamma_{\text{adh}} = \gamma_{\text{coh}}$), it increases to 50% in the case of the reduced adhesion ($\gamma_{\text{adh}} = 0.6\gamma_{\text{coh}}$).

The effect of adhesion on the internal morphology of the wear particle can be discussed by arguing that a stronger adhesion promotes a deeper propagation of subsurface cracks and a larger removal of surface material during particle formation. In other words, a thicker layer of subsurface material transfers to the rolling particle when a strong adhesion is present between sliding surfaces. This observation can be understood by analyzing the state of stresses at the contact between the rolling particle and sliding surfaces.

Considering a simple 2D stress state [Fig. 5(a)], the angle of the maximum principal stress, that is responsible for the subsurface crack propagation at the trailing edge of the rolling wear particle, can be computed as

$$\theta_I = 0.5\,\tan^{-1}\left(\frac{2\tau_j}{\sigma}\right), \tag{3}$$

where σ and τ_j are the normal and shear stresses at the contact between the rolling particle and the sliding surfaces. For a given size of the rolling particle and under a constant applied load, one can assumes a constant normal stress at the contact. In this situation, a larger interfacial adhesion causes a higher contact shear strength (τ_j) and the angle of maximum principal stress (θ_I), resulting a deeper propagation of subsurface cracks. Comparing Figs. 5(b) and 5(c), it evidents that the stronger the interfacial adhesion, the deeper the propagation of subsurface cracks and the larger the amount of removed material. A similar argument was hypothesized in the Suh's delamination theory of wear [24] that the increase in surface traction (and the tangential component of contact stresses) can create thicker wear particles, causing the transition from mild to severe wear.

This analysis may also rationalized the existence of surface asperities with larger aspect ratios at smaller scales [60,61]. At smaller scales, the probability of cold welding (due to severe plastic yielding) and formation of high shear strength junctions between surface asperities is higher. As a result,

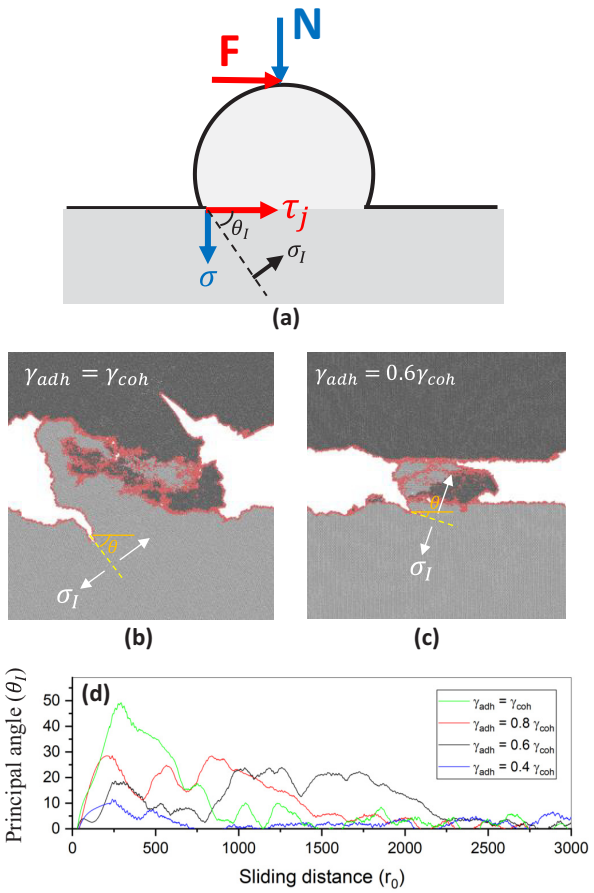

FIG. 5. (a) Schematic of stress state at the contact between the rolling third body particle and sliding surface. The angle of subsurface crack propagation in adhesive wear simulations with (b) full ($\gamma_{\text{adh}} = \gamma_{\text{coh}}$) and (c) reduced ($\gamma_{\text{adh}} = 0.6\gamma_{\text{coh}}$) interfacial adhesion, showing that the stronger the interfacial adhesion, the deeper the crack propagation angle and the larger the amount of removal material. (d) Evolution of the angle of maximum principal stress (θ_I) at the trailing edge of the rolling wear particles.

deeper subsurface cracks and thus a higher surface roughness can be expected at smaller scales.

Figure 5(d) shows the evolution of (θ_I) as a function of sliding distance for different adhesion coefficients. As seen, the crack opening angle is the largest in the simulation with the full interfacial adhesion. This analysis explains abrupt formation of a wear particle over a short sliding distance in the presence of strong adhesion. It explains also why the system reaches to a steady state in terms of wear particle size and tangential force as θ_I and consequently the amount of transferred material from the sliding surfaces to the rolling particle diminish [Fig. 4(g)]. The reduction of θ_I over the sliding distance can be explained as the interfacial shear strength between the particle and sliding surfaces decreases due to the surface contamination and imperfect contact geometry between the rolling particle and sliding surfaces.

IV. CONCLUSION

By developing a new algorithm to model the effect of chemically driven surface contamination in molecular dynamic simulations, we studied a complete process of nucleation, evolution and detachment of a wear particle during adhesive wear. Our simulations confirm a long-standing hypothesis [1,24,31] of wear particle formation by agglomeration of transferred material fragments. Our simulations revealed that in the presence of a strong adhesion, wear particles are formed through the agglomeration of a few but instantaneously removed large fragments over a small sliding distance. On the contrary, the weak adhesion promotes the mild formation of smaller particles through the accretion of flake-like transferred sheets. Our simulations highlight different contributions of interfacial adhesion during the process of wear particle formation. It demonstrates that reducing adhesion (i) decreases the probability of wear particle formation at the asperity contact (confirming the critical junction size model [9] [Eq. (1)]), (ii) reduces the size of loose wear particle (in agreement with previous experimental observations [5,48]), and decreases the energy efficiency of material removal process (i.e., the lower the adhesion, the amount of energy required is higher to remove a unit volume of surface material).

ACKNOWLEDGMENTS

The author acknowledges financial support from the Aarhus University Research Foundation, AUFF (Grant No. 27236, "Microscopic origins of adhesive wear"). This work was made possible by usage of computing resources at the ETAIS (Estonian Scientific Computing Infrastructure) through the NeIC Dellingr resource sharing pilot and the Prime cluster at the Department of Engineering, Aarhus University.

[1] T. Sasada, S. Norose, and H. Mishina, J. Lubr. Technol. **103**, 195 (1981).
[2] E. Rabinowicz, *Friction and Wear of Materials* (Wiley, 1995), Chap. 5, pp. 125–166.
[3] Q. Li, R. Pohrt, and V. L. Popov, Front. Mech. Eng. **5**, 7 (2019).
[4] D. Buckley, *Surface Effects in Adhesion, Friction, Wear, and Lubrication* (Elsevier, 1981), Chap. 5, pp. 245–313.
[5] K. Hiratsuka, Tribol. Int. **28**, 279 (1995).
[6] T. Kuwahara, G. Moras, and M. Moseler, Phys. Rev. Mater. **2**, 073606 (2018).
[7] P. Stoyanov, P. Stemmer, T. T. Järvi, R. Merz, P. A. Romero, M. Scherge, M. Kopnarski, M. Moseler, A. Fischer, and M. Dienwiebel, ACS Appl. Mater. Interfaces **5**, 6123 (2013).
[8] P. A. Romero, T. T. Järvi, N. Beckmann, M. Mrovec, and M. Moseler, Phys. Rev. Lett. **113**, 036101 (2014).
[9] R. Aghababaei, D. H. Warner, and J.-F. Molinari, Nat. Commun. **7**, 11816 (2016).
[10] E. Milanese, T. Brink, R. Aghababaei, and J.-F. Molinari, Nat. Commun. **10**, 1116 (2019).
[11] K. N. G. Fuller and D. Tabor, Proc. R. Soc. London A **345**, 327 (1975).
[12] B. N. J. Persson and E. Tosatti, J. Chem. Phys. **115**, 5597 (2001).
[13] L. Pastewka and M. O. Robbins, Proc. Natl. Acad. Sci. U. S. A. **111**, 3298 (2014).
[14] V. L. Popov, R. Pohrt, and Q. Li, Friction **5**, 308 (2017).
[15] N. P. Suh, N. Saka, and S. Jahanmir, Wear **44**, 127 (1977).
[16] J. Fontaine, C. Donnet, and A. Erdemir, Fundamentals of the tribology of dlc coatings, in *Tribology of Diamond-Like Carbon Films: Fundamentals and Applications*, edited by C. Donnet and A. Erdemir (Springer US, Boston, MA, 2008), pp. 139–154.
[17] M. D. B. Bouchet, C. Matta, B. Vacher, T. Le-Mogne, J. Martin, J. von Lautz, T. Ma, L. Pastewka, J. Otschik, P. Gumbsch, and M. Moseler, Carbon **87**, 317 (2015).
[18] F. P. Bowden and D. Tabor, Proc. R. Soc. London A **169**, 391 (1939).
[19] M. Cocks, J. Appl. Phys. **29**, 1609 (1958).
[20] I. Feng, J. Appl. Phys. **23**, 1011 (1952).
[21] J. F. Archard, J. Appl. Phys. **24**, 981 (1953).
[22] H.-C. Sin and N. P. Suh, J. Appl. Mech. **51**, 317 (1984).
[23] K. Komvopoulos and S.-S. Cho, Wear **209**, 57 (1997).
[24] N. P. Suh, Wear **25**, 111 (1973).
[25] J. Fleming and N. Suh, Wear **44**, 39 (1977).
[26] K. Kato, Wear **153**, 277 (1992).
[27] M. Godet, Wear **100**, 437 (1984).
[28] K. Hiratsuka and K. Muramoto, Wear **259**, 467 (2005), 15th International Conference on Wear of Materials.
[29] I. M. Hutchings, Wear **360-361**, 51 (2016).
[30] M. Kerridge and J. K. Lancaster, Proc. R. Soc. London A **236**, 250 (1956).
[31] G. Stachowiak and A. Batchelor, *Engineering Tribology*, 3rd ed. (Elsevier, 1993), Chap. 12, pp. 613–635.
[32] T. Sato, T. Ishida, L. Jalabert, and H. Fujita, Nanotechnology **23**, 505701 (2012).
[33] L. M. Keer, Y. Xu, H. S. Cheng, and J. L. Xuan, Tribol. Trans. **36**, 613 (1993).
[34] P. Ko, S. Iyer, H. Vaughan, and M. Gadala, Wear **251**, 1265 (2001).
[35] A. Akchurin, R. Bosman, and P. M. Lugt, Tribol. Int. **110**, 201 (2017).
[36] V. L. Popov and R. Pohrt, Friction **6**, 260 (2018).
[37] R. Aghababaei, D. H. Warner, and J.-F. Molinari, Proc. Natl. Acad. Sci. U. S. A. **114**, 7935 (2017).

[38] R. Aghababaei, T. Brink, and J.-F. Molinari, Phys. Rev. Lett. **120**, 186105 (2018).
[39] R. Aghababaei, Wear **426-427**, 1076 (2019), 22nd International Conference on Wear of Materials.
[40] A. A. Griffith, Philos. Trans. R. Soc. London A **221**, 163 (1921).
[41] E. Orowan, Rep. Prog. Phys. **12**, 185 (1949).
[42] L. Frérot, R. Aghababaei, and J.-F. Molinari, J. Mech. Phys. Solids **114**, 172 (2018).
[43] M. H. Müser and A. Wang, Lubricants **6**, 85 (2018).
[44] T. Brink and J.-F. Molinari, Phys. Rev. Mater. **3**, 053604 (2019).
[45] M. Cocks, J. Appl. Phys. **35**, 1807 (1964).
[46] E. Rabinowicz, Wear **7**, 9 (1964).
[47] S. Zaghdoudi and R. J. Gibert, *Wear Particles: From the Cradle to the Grave* (Elsevier Science, Netherland, 1992), Chap. 3, pp. 57–145.
[48] E. Rabinowicz, Wear **2**, 4 (1958).
[49] E. Rabinowicz, J. Appl. Phys. **32**, 1440 (1961).
[50] E. Popova, V. L. Popov, and D.-E. Kim, Friction **6**, 341 (2018).
[51] P. M. Morse, Phys. Rev. **34**, 57 (1929).
[52] See Supplemental Material at http://link.aps.org/supplemental/10.1103/PhysRevMaterials.3.063604 for movie of simulations, presented in Fig. 2.
[53] S. Plimpton, J. Comput. Phys. **117**, 1 (1995).
[54] A. Stukowski, Modell. Simul. Mater. Sci. Eng. **18**, 015012 (2010).
[55] S. Danyluk, M. McNallan, and D. S. Park, *Friction and Wear of Ceramics* (Elsevier, 1993), Chap. 2, pp. 15–99.
[56] X. Chen, Rock friction and dynamic faulting at the micro- to nano-scales, Ph.D. thesis, University of Oklahoma, 2015.
[57] Z. Reches and D. A. Lockner, Nature (London) **467**, 452 (2010).
[58] N. P. Suh, Wear **44**, 1 (1977).
[59] D. Scott and G. Mills, Wear **24**, 235 (1973).
[60] E. E. Brodsky, J. D. Kirkpatrick, and T. Candela, Geology **44**, 19 (2016).
[61] T. Candela and E. E. Brodsky, Geology **44**, 603 (2016).